# TWO-DIMENSIONAL X-RAY DIFFRACTION

BOB B. HE

WILEY
A JOHN WILEY & SONS, INC., PUBLICATION

# TWO-DIMENSIONAL X-RAY DIFFRACTION

# TWO-DIMENSIONAL X-RAY DIFFRACTION

BOB B. HE

WILEY
A JOHN WILEY & SONS, INC., PUBLICATION

Published by John Wiley & Sons, Inc., Hoboken, New Jersey
Published simultaneously in Canada



***Library of Congress Cataloging-in-Publication Data:***

He, Bob B., 1954 –
Two-dimensional X-ray diffraction / Bob B. He.
p. cm.
Includes index.
ISBN 978-0-470-22722-0 (cloth)
1. X-rays – Diffraction. 2. X-rays – Diffraction – Experiments. 3. X-rays – Diffraction – Industrial applications. I. Title.
QC482.D5H4 2009
548′.83 – dc22

2009005619

Printed in the United States of America.

10 9 8 7 6 5 4 3 2 1

# CONTENTS

**Preface** **xiii**

**1. Introduction** **1**

1.1 X-Ray Technology and Its Brief History, 1
1.2 Geometry of Crystals, 2
1.2.1 Crystal Lattice and Symmetry, 3
1.2.2 Lattice Directions and Planes, 4
1.2.3 Atomic Arrangement in Crystal Structure, 9
1.2.4 Imperfections in Crystal Structure, 11
1.3 Principles of X-Ray Diffraction, 13
1.3.1 Bragg Law, 13
1.3.2 Diffraction Patterns, 14
1.4 Reciprocal Space and Diffraction, 16
1.4.1 Reciprocal Lattice, 16
1.4.2 The Ewald Sphere, 18
1.4.3 Diffraction Cone and Diffraction Vector Cone, 19
1.5 Two-Dimensional X-Ray Diffraction, 21
1.5.1 Diffraction Pattern Measured by Area Detector, 21
1.5.2 Two-Dimensional X-Ray Diffraction System and Major Components, 22
1.5.3 Summary, 23
References, 25

**2. Geometry Conventions** **28**

2.1 Introduction, 28
2.1.1 Comparison Between XRD$^2$ and Conventional XRD, 29
2.2 Diffraction Space and Laboratory Coordinates, 30
2.2.1 Diffraction Cones in Laboratory Coordinates, 30
2.2.2 Diffraction Vector Cones in Laboratory Coordinates, 33
2.3 Detector Space and Detector Geometry, 35
2.3.1 Ideal Detector for Diffraction Pattern in 3D Space, 35
2.3.2 Diffraction Cones and Conic Sections with Flat 2D Detectors, 36
2.3.3 Detector Position in the Laboratory System, 37
2.3.4 Pixel Position in Diffraction Space—Flat Detector, 37
2.3.5 Pixel Position in Diffraction Space—Curved Detector, 39
2.4 Sample Space and Goniometer Geometry, 42
2.4.1 Sample Rotations and Translations in Eulerian Geometry, 42
2.4.2 Variation of Goniometer Geometry, 44
2.5 Transformation from Diffraction Space to Sample Space, 46
2.6 Summary of XRD$^2$ Geometry, 49
References, 49

**3. X-Ray Source and Optics** **51**

3.1 X-Ray Generation and Characteristics, 51
3.1.1 X-Ray Spectrum and Characteristic Lines, 51
3.1.2 Focal Spot and Takeoff Angle, 53
3.1.3 Focal Spot Brightness and Profile, 53
3.1.4 Absorption and Fluorescence, 55
3.2 X-Ray Optics, 56
3.2.1 Liouville's Theorem and Fundamentals, 56
3.2.2 X-Ray Optics in a Conventional Diffractometer, 59
3.2.3 X-Ray Optics in Two-Dimensional Diffractometer, 62
3.2.4 The β-Filter, 66
3.2.5 Crystal Monochromator, 68
3.2.6 Multilayer Mirrors, 70
3.2.7 Pinhole Collimator, 76
3.2.8 Capillary Optics, 79
References, 83

**4. X-Ray Detectors** **85**

4.1 History of X-Ray Detection Technology, 85
4.2 Point Detectors in Conventional Diffractometers, 88
4.2.1 Proportional Counters, 88
4.2.2 Scintillation Counters, 89
4.2.3 Solid-State Detectors, 90

4.3 Characteristics of Point Detectors, 91
4.3.1 Counting Statistics, 91
4.3.2 Detective Quantum Efficiency and Energy Range, 93
4.3.3 Detector Linearity and Maximum Count Rate, 94
4.3.4 Energy Resolution, 96
4.3.5 Detection Limit and Dynamic Range, 98
4.4 Line Detectors, 100
4.4.1 Geometry of Line Detectors, 100
4.4.2 Types of Line Detectors, 103
4.4.3 Characteristics of Line Detectors, 104
4.5 Characteristics of Area Detectors, 107
4.5.1 Geometry of Area Detectors, 108
4.5.2 Spatial Resolution of Area Detectors, 112
4.6 Types of Area Detectors, 114
4.6.1 Multiwire Proportional Counter, 115
4.6.2 Image Plate, 117
4.6.3 CCD Detector, 118
4.6.4 Microgap Detector, 122
4.6.5 Comparison of Area Detectors, 127
References, 130

**5. Goniometer and Sample Stages 133**

5.1 Goniometer and Sample Position, 133
5.1.1 Introduction, 133
5.1.2 Two-Circle Base Goniometer, 134
5.1.3 Sample Stages, 135
5.1.4 Sequence of the Goniometer Axes, 136
5.2 Goniometer Accuracy, 138
5.2.1 Sphere of Confusion, 138
5.2.2 Angular Accuracy and Precision, 141
5.3 Sample Alignment and Visualization Systems, 143
5.4 Environment Stages, 145
5.4.1 Domed High Temperature Stage, 145
5.4.2 Temperature Stage Calibration, 146
References, 149

**6. Data Treatment 151**

6.1 Introduction, 151
6.2 Nonuniform Response Correction, 151
6.2.1 Calibration Source, 152
6.2.2 Nonuniform Response Correction Algorithms, 154
6.3 Spatial Correction, 156
6.3.1 Fiducial Plate and Detector Plane, 156
6.3.2 Spatial Correction Algorithms, 158

6.4 Detector Position Accuracy and Calibration, 163
6.4.1 Detector Position Tolerance, 163
6.4.2 Detector Position Calibration, 165
6.5 Frame Integration, 167
6.5.1 Definition of Frame Integration, 167
6.5.2 Algorithm of Frame Integration, 170
6.6 Lorentz, Polarization, and Absorption Corrections, 175
6.6.1 Lorentz, 175
6.6.2 Polarization, 176
6.6.3 Air Scatter and Be-Window Absorption, 180
6.6.4 Sample Absorption, 182
6.6.5 Combined Intensity Correction, 188
References, 189

**7. Phase Identification** **191**

7.1 Introduction, 191
7.2 Relative Intensity, 193
7.2.1 Multiplicity Factor, 193
7.2.2 Electron and Atomic Scattering, 194
7.2.3 Structure Factor, 196
7.2.4 Attenuation Factors, 197
7.3 Geometry and Resolution, 197
7.3.1 Detector Distance and Resolution, 198
7.3.2 Defocusing Effect, 199
7.3.3 Transmission Mode Diffraction, 201
7.4 Sampling Statistics, 202
7.4.1 Effective Sampling Volume, 203
7.4.2 Angular Window, 204
7.4.3 Virtual Oscillation, 205
7.4.4 Sample Oscillation, 206
7.5 Preferred Orientation Effect, 208
7.5.1 Relative Intensity with Texture, 208
7.5.2 Intensity Correction on Fiber Texture, 211
References, 216

**8. Texture Analysis** **218**

8.1 Introduction, 218
8.2 Pole Density and Pole Figure, 219
8.3 Fundamental Equations, 222
8.3.1 Pole Figure Angles, 222
8.3.2 Pole Density, 224
8.4 Data Collection Strategy, 225
8.4.1 Single Scan, 225
8.4.2 Multiple Scan, 227
8.4.3 Comparison with Point Detector, 230

8.5 Texture Data Process, 231
8.5.1 $2\theta$ Integration, 231
8.5.2 Absorption Correction, 234
8.5.3 Pole Figure Interpolation, 235
8.5.4 Pole Figure Symmetry, 235
8.5.5 Pole Figure Normalization, 237
8.6 Orientation Distribution Function, 237
8.6.1 Eulerian Angles and Space, 237
8.6.2 ODF Calculation, 239
8.6.3 Calculated Pole Figures From ODF, 241
8.7 Fiber Texture, 242
8.7.1 Pole Figures of Fiber Texture, 242
8.7.2 ODF of Fiber Texture, 244
8.8 Other Advantages of XRD$^2$ for Texture, 244
8.8.1 Orientation Relationship, 245
8.8.2 Direct Observation of Texture, 245
References, 247

**9. Stress Measurement 249**

9.1 Introduction, 249
9.1.1 Stress, 250
9.1.2 Strain, 254
9.1.3 Elasticity and Hooke's Law, 256
9.1.4 X-Ray Elasticity Constants and Anisotropy Factor, 257
9.1.5 Residual Stresses, 258
9.2 Principle of X-Ray Stress Analysis, 260
9.2.1 Strain and Bragg Law, 260
9.2.2 Strain Measurement, 261
9.2.3 Stress Measurement, 263
9.2.4 Stress Measurement Without $d_0$, 266
9.2.5 $\psi$-Tilt and Goniometer, 269
9.2.6 $\mathrm{Sin}^2\psi$ Method with Area Detector, 270
9.3 Theory of Stress Analysis with XRD$^2$, 272
9.3.1 2D Fundamental Equation for Stress Measurement, 272
9.3.2 Relationship Between Conventional Theory and 2D Theory, 276
9.3.3 2D Equations for Various Stress States, 278
9.3.4 True Stress-Free Lattice $d$-Spacing, 280
9.3.5 Diffraction Cone Distortion Simulation, 281
9.4 Process of Stress Measurement with XRD$^2$, 288
9.4.1 Instrument Requirements and Configurations, 288
9.4.2 Data Collection Strategy, 291
9.4.3 Data Integration and Peak Evaluation, 295
9.4.4 Stress Calculation, 299
9.4.5 Intensity Weighted Least Squares Regression, 300

9.5 Experimental Examples, 303
9.5.1 Comparison Between 2D Method and Conventional Method, 303
9.5.2 Virtual Oscillation for Stress Measurement, 305
9.5.3 Stress Mapping on Weldment, 307
9.5.4 Residual Stresses in Thin Films, 310
9.5.5 Residual Stress Measurement with Multiple {*hkl*} Rings, 315
9.5.6 Gage Repeatability and Reproducibility Study, 316
Appendix 9.A Calculation of Principal Stresses from the General Stress Tensor, 320
Appendix 9.B Parameters for Stress Measurement, 323
References, 325

**10. Small-Angle X-Ray Scattering 329**

10.1 Introduction, 329
10.1.1 Principle of Small-Angle Scattering, 330
10.1.2 General Equation and Parameters in SAXS, 330
10.1.3 X-Ray Source and Optics for SAXS, 331
10.2 2D SAXS Systems, 333
10.2.1 SAXS Attachments, 334
10.2.2 Dedicated SAXS System, 336
10.2.3 Detector Correction and System Calibration, 337
10.2.4 Data Collection and Integration, 338
10.3 Application Examples, 341
10.3.1 Particles in Solutions, 341
10.3.2 Scanning SAXS and Transmission Measurement, 341
10.4 Some Innovations in 2D SAXS, 343
10.4.1 Simultaneous Measurements of Transmission and SAXS, 343
10.4.2 Vertical SAXS System, 346
References, 347

**11. Combinatorial Screening 351**

11.1 Introduction, 351
11.1.1 Combinatorial Chemistry, 351
11.1.2 Combinatorial Screening, 352
11.2 $XRD^2$ Systems for Combinatorial Screening, 352
11.2.1 Combinatorial Screening in Reflection Geometry, 353
11.2.2 Retractable Knife-Edge, 356
11.2.3 Combinatorial Screening in Transmission Geometry, 359
11.3 Combined Screening with $XRD^2$ and Raman, 364
References, 366

**12. Quantitative Analysis** **369**

12.1 Percent Crystallinity, 369
12.1.1 Introduction, 369
12.1.2 Comparison of Conventional XRD and XRD$^2$, 370
12.1.3 Scatter Correction, 371
12.1.4 Internal and External Methods, 373
12.1.5 Full Method, 374
12.2 Crystal Size, 376
12.2.1 Introduction, 376
12.2.2 Line Broadening for Crystallite Size, 377
12.2.3 $\gamma$-Profile Analysis for Crystallite Size, 380
12.3 Retained Austenite, 387
References, 390

**13. Innovation and Future Development** **393**

13.1 Introduction, 393
13.2 Scanning Line Detector for XRD$^2$, 394
13.2.1 Working Principle, 394
13.2.2 Advantages of Scanning Line Detector, 396
13.3 Three-Dimensional Detector, 398
13.3.1 The Third Dimension of a Detector, 398
13.3.2 Geometry of Three-Dimensional Detector, 399
13.3.3 Three-Dimensional Detector and Reciprocal Space, 401
13.4 Pixel Direct Diffraction Analysis, 402
13.4.1 Concept, 402
13.4.2 Pixel Diffraction Vector and Pixel Count, 403
13.4.3 PDD Analysis in Phase-ID, Texture, and Stress, 404
References, 406

**Appendix A. Values of Commonly Used Parameters** **407**

**Appendix B. Symbols** **412**

**Index** **419**

# PREFACE

Two-dimensional X-ray diffraction is the ideal, nondestructive, analytical method for examining samples of many types, such as metals, polymers, ceramics, semiconductors, thin films, coatings, paints, biomaterials and composites for material science researches, molecular structure determination and polymorphism study for drug discovery and processing, and samples with microvolume or microarea for forensic analysis, archeological analysis, and many emerging applications. In the long history of powder X-ray diffraction, data collection and analysis have been based mainly on one-dimensional diffraction profiles measured with scanning point detectors or linear position-sensitive detectors. Therefore, almost all X-ray powder diffraction applications, such as phase identification, texture, residual stress, crystallite size, and percent crystallinity are developed in accord with the diffraction profiles collected by conventional diffractometers. A two-dimensional diffraction pattern contains abundant information about the atomic arrangement, microstructure, and defects of a solid or liquid material. Because of the unique nature of the data collected with an area detector, many algorithms and methods developed for conventional X-ray diffraction are not sufficient or accurate to interpret and analyze the data from two-dimensional X-ray diffraction. New concepts and approaches are necessary to design a two-dimensional diffractometer and to understand and analyze two-dimensional diffraction data. In addition, the new theory should also be consistent with conventional theory because two-dimensional X-ray diffraction is also a natural extension of conventional X-ray diffraction.

The purpose of this book is to give an introduction to two-dimensional X-ray diffraction. Chapter 1 gives a brief introduction to X-ray diffraction and its extension to two-dimensional X-ray diffraction. Content on the general principles of diffraction is kept to a minimum since many books on the subject are available. The geometry

conventions and diffraction vector analysis in Chapter 2 provide the foundation for the subjects discussed in the following chapters. Chapters 3 to 6 focus on the instrumentation technologies, including the critical components, system configurations, and basic data collection and process algorithms. Chapters 7–13 introduce the basic concepts, diffractometer configurations, data collection strategy, data analysis algorithm, and experimental examples for various applications, such as phase identification, texture, stress, microstructure analysis, crystallinity, thin film analysis, and combinatorial screening.

Writing my first book in my second language is like swimming without knowing the depth of the water. I am glad that the struggle in my heart between the desire and hesitation to write this book is finally over, thanks so much for the encouragement and help from many colleagues and friends. I would like to express my sincere appreciation to Professors Mingzhi Huang, Huijiu Zhou, Jiawen He, Charles Houska, Guoquan Lu, and Robert Hendricks for their guidance, assistance, and encouragement in my education and career development. I wish to acknowledge the support, suggestions, and contributions from my colleagues, especially from Kingsley Smith, Uwe Preckwinkel, Roger Durst, Yacouba Diawara, John Chambers, Gary Schmidt, Mike Mott, Kerry Klitzke, Dave Teasdale, James Neuenfeldt, Sue Byram, Chuck Campana, Michael Ruf, Joerg Kaercher, Pete MaDonald, Randy Heimann, Beth Beutler, Bruce Becker, Brian Michell, Jerry Schwarz, Greg Wachter, Kline Wilkins, Heiko Ress, Peter LaPuma, Lutz Brügemann, Frank Burgäzy, Hannes Jakob, Kurt Helming, Arnt Kern, Alexander Ulyanenkov, Jens Brechbuehl, Keisuke Saito, Detlef Bahr, and Kurt Erlacher. I am grateful to those who have so generously contributed their ideas, inspiration, and insights through many thoughtful discussions and communications, particularly to Thomas Blanton, Davor Balzar, Camden Hubbard, James Britten, Joseph Reibenspies, Ralph Tissot, Herbert Goebel, Joseph Formica, Richard Ortega, Brian Litteer, Jian Lu, Xun-Li Wang, John Anzelmo, Brian Toby, Ting Huang, Alejandro Navarro, Kewei Xu, Berthold Scholtes, Gregory Stephenson, Raj Suryanarayanan, Shawn Yin, Chris Frampton, Chris Gilmore, Keisuke Tanaka, Wulf Pfeiffer, Dierk Raabe, Robert Snyder, Jose Miguel Delgado, Winnie Wong-Ng, Xiaolong Chen, Weimin Mao, Kun Tao, Dulal Goldar, Vincent Ji, Peter Lee, Yan Gao, Fangling Needham, Timothy Fawcett, James Kaduk, and John Faber. I am indebted to my wife Judy for her patience, care, and understanding and my son Mike for his support.

Serving as Director of R&D for Bruker AXS, an industry leader in X-ray diffraction instrumentation, gives me the opportunity to meet many scientists, engineers, professors, and students working in the field of X-ray diffraction, and the resources to put many ideas into practice. The many pictures and experimental data in this book are collected from the diffractometers manufactured by Bruker AXS, Inc. This should not be considered as an endorsement of a particular vendor, rather a convenient way to express the ideas. The approaches and algorithms suggested in this book are not necessarily the best alternatives and some errors may exist due to my mistakes. I welcome any comments, suggestions, and criticisms.

BOB BAOPING HE

# 1

# INTRODUCTION

## 1.1 X-RAY TECHNOLOGY AND ITS BRIEF HISTORY

X-ray technology has more than a hundred years of history and its discovery and development has revolutionized many areas of modern science and technology [1]. X-rays were discovered by the German physicist Wilhelm Conrad Röntgen in 1895, who was honored with the Nobel Prize for Physics in 1901. In many languages today, X-rays are still referred to as Röntgen rays or Röntgen radiation. The mysterious light was found to be invisible to human eyes, but capable of penetrating opaque objects and exposing photographic films. The density contrast of the object is revealed on the developed film as a radiograph. Since then, X-rays have been developed for medical imaging, for example, for detection of bony structures and diseases in soft tissues such as pneumonia and lung cancer. X-rays have also been used to treat diseases. Radiotherapy employs high-energy X-rays to generate a curative medical intervention to the cancer tissues. A recent technology, tomotherapy, combines the precision of a computerized tomography scan with the potency of radiation treatment to selectively destroy cancerous tumors while minimizing damage to surrounding tissue. Today, medical diagnoses and treatments are still the most common use of X-ray technology.

The phenomenon of X-ray diffraction by crystals was discovered in 1912 by Max von Laue. The diffraction condition in a simple mathematical form, which is now known as the Bragg law, was formulated by Lawrence Bragg in the same year. The Nobel Prizes for Physics in two consecutive years (1914 and 1915) were awarded

*Two-Dimensional X-Ray Diffraction* By Bob B. He

to von Laue and the senior and junior Bragg for the discovery and explanation of X-ray diffraction. X-ray diffraction techniques are based on elastic scattered X-rays from matter. Due to the wave nature of X-rays, the scattered X-rays from a sample can interfere with each other such that the intensity distribution is determined by the wavelength and the incident angle of the X-rays and the atomic arrangement of the sample structure, particularly the long-range order of crystalline structures. The expression of the space distribution of the scattered X-rays is referred to as an X-ray diffraction pattern. The atomic level structure of the material can then be determined by analyzing the diffraction pattern. Over its hundred-year history of development, X-ray diffraction techniques have evolved into many specialized areas. Each has its specialized instruments, samples of interests, theory, and practice. Single-crystal X-ray diffraction (SCD) is a technique used to solve the complete structure of crystalline materials, typically in the form of single crystals. The technique started with simple inorganic solids and grew into complex macromolecules. Protein structures were first determined by X-ray diffraction analysis by Max Perutz and Sir John Cowdery Kendrew in 1958 and both shared the 1962 Nobel Prize in Chemistry. Today, protein crystallography is the dominant application of SCD. X-ray powder diffraction (XRPD), alternatively powder X-ray diffraction (PXRD), got its name from the technique of collecting X-ray diffraction patterns from packed powder samples. Generally, X-ray powder diffraction involves the characterization of the crystallographic structure, crystallite size, and orientation distribution in polycrystalline samples [2–5].

X-ray diffraction (XRD), by definition, covers single-crystal diffraction and powder diffraction as well as many X-ray diffraction techniques. However, it has been accepted as convention that SCD is distinguished from XRD. By this practice, XRD is commonly used to represent various X-ray diffraction applications other than SCD. These applications include phase identification, texture analysis, stress measurement, percent crystallinity, particle (grain) size, and thin film analysis. An analogous method to X-ray diffraction is small-angle X-ray scattering (SAXS) technique. SAXS measures scattering intensity at scattering angles within a few degrees from the incident angle. SAXS pattern reveals the material structures, typically particle size and shape, in the nanometer to micrometer range. In contrast to SAXS, other X-ray diffraction techniques are also referred to as wide-angle X-ray scattering (WAXS).

## 1.2 GEOMETRY OF CRYSTALS

Solids can be divided into two categories: amorphous and crystalline. In an amorphous solid, glass, for example, atoms are not arranged with long-range order. Thus, amorphous solids are also referred to as “glassy” solids. In contrast, a crystal is a solid formed by atoms, molecules, or ions stacking in three-dimensional space with a regular and repeating arrangement. The geometry and structure of a crystalline solid determines the X-ray diffraction pattern. Comprehensive knowledge of crystallography has been covered by many books [2,5–9]. This section gives only some basics to help further discussion on X-ray diffraction.

### 1.2.1 Crystal Lattice and Symmetry

A crystal structure can be simply expressed by a point lattice as shown in Figure 1.1(a). The point lattice represents the three-dimensional arrangement of the atoms in the crystal structure. It can be imagined as being comprised of three sets of planes, each set containing parallel crystal planes with equal interplane distance. Each intersection of three planes is called lattice point and represents the location of the center of an atom, ion, or molecule in the crystal. A point lattice can be minimally represented by a unit cell, highlighted in bold in the bottom left corner. A complete point lattice can be formed by the translation of the unit cell in three-dimensional space. This feature is also referred to as translation symmetry. The shape and size of a unit cell can be defined by three vectors **a**, **b**, and **c** all starting from any single lattice point as shown in Figure 1.1(b). The three vectors are called the crystallographic axes of the cell. As each vector can be defined by its length and direction, a unit cell can also be defined by the three lengths of the vectors ($a$, $b$, and $c$) as well as the angles between them ($\alpha$, $\beta$, and $\gamma$). The six parameters ($a$, $b$, $c$, $\alpha$, $\beta$, and $\gamma$) are referred to as the lattice constants or lattice parameters of the unit cell.

One important feature of crystals is their symmetry. In addition to the translation symmetry in point lattices, there are also four basic point symmetries: reflection, rotation, inversion, and rotation–inversion. Figure 1.2 shows all four basic point symmetries on a cubic unit cell. The reflection plane is like a mirror. The reflection plane divides the crystal into two sides. Each side of the crystal matches the mirrored position of the other side. The cubic structure has several reflection planes. The rotation axes include two-, three-, four-, and sixfold axes. A rotation of a crystal about an $n$-fold axis by $360°/n$ will bring it into self-coincidence. A cubic unit cell has several two-, three- and fourfold axes. The inversion center is like a pinhole camera; the crystal will maintain self-coincidence if every point of the crystal inverted through the inversion center. Any straight line passing through the inversion center intersects with the same lattice point at the same distance at both sides of the inversion center. A cubic unit cell has an inversion center in its body center. The rotation–inversion center can be considered as a combined symmetry of rotation and inversion.

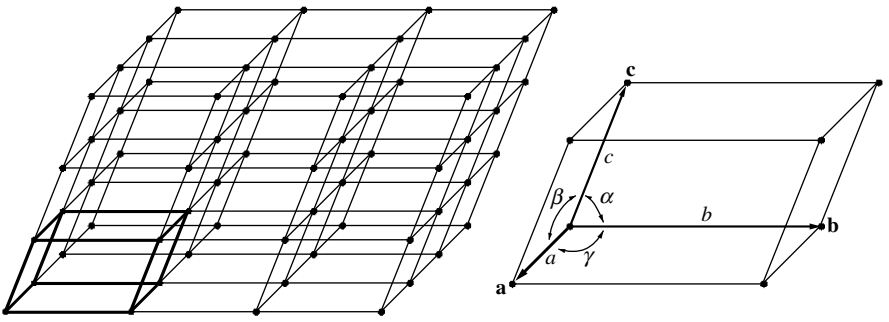


**FIGURE 1.1** A point lattice (a) and its unit cell (b).

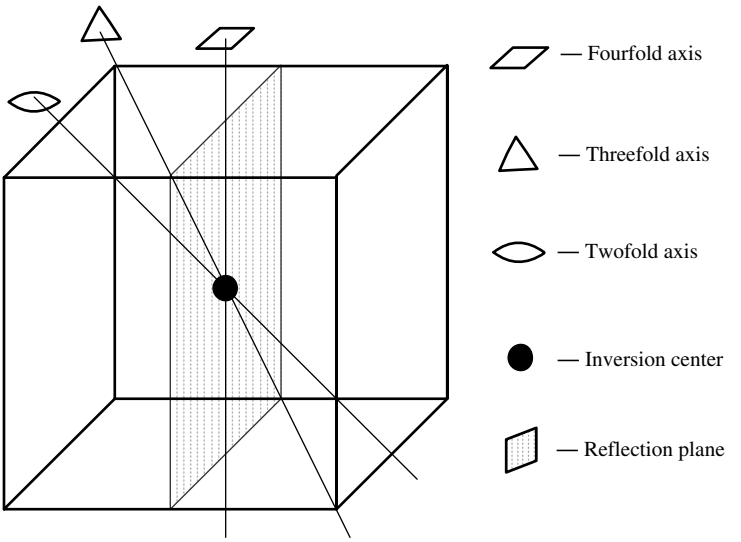


**FIGURE 1.2** Symmetry elements of a cubic unit cell.

The various relationships among the six lattice parameters ($a$, $b$, $c$, $\alpha$, $\beta$, and $\gamma$) result in various crystal systems. The simplest crystal system is cubic system in which all three crystallographic vectors are equal in length and perpendicular to each other ($a = b = c$ and $\alpha = \beta = \gamma = 90°$). Seven crystal systems are sufficient to cover all possible point lattices. The French crystallographer Bravais found that there are a total of 14 possible point lattices. Seven point lattices are given by the seven crystal systems for the case that only one lattice point is in each unit cell and that the lattice point is located in the corner of the unit cell. These seven types of unit cells are called primitive cells and labeled by P or R. By adding one or more lattice points within a unit cell, one can create nonprimitive cells depending on the location of the additional lattice points. The location of a lattice point in the unit cell can be specified by fractional coordinates within a unit cell ($u$, $v$, $w$). For example, the lattice point in a primitive cell is (0, 0, 0). Therefore, we can define three types of nonprimitive cells. The label I represents the body-centered point lattice, which has one additional lattice point at the center of the unit cell, or can be defined by the fraction ($\frac{1}{2}$, $\frac{1}{2}$, $\frac{1}{2}$). The label F represents the face-centered point lattice with additional lattice points at the center of unit cell face, or (0, $\frac{1}{2}$, $\frac{1}{2}$), ($\frac{1}{2}$, 0, $\frac{1}{2}$), and ($\frac{1}{2}$, $\frac{1}{2}$, 0). The label C represents the base-centered point lattice with an additional lattice point at the center of the base face ($\frac{1}{2}$, $\frac{1}{2}$, 0). All 7 crystal systems and 14 Bravais lattices are summarized in Table 1.1. The unit cells of the 14 Bravais lattices are shown in Figure 1.3.

### 1.2.2 Lattice Directions and Planes

The direction of any line in a crystal lattice can be specified by drawing a line starting from the unit cell origin parallel to the given line and then taking the

**TABLE 1.1 Crystal Systems and Bravais Lattices**

| The Seven Crystal Systems | Unit Cell | Minimum Symmetry | Bravais Lattices | Lattice Symbol |
|---|---|---|---|---|
| Cubic | $\alpha=\beta=\gamma=90^\circ$<br>$a=b=c$ | Four threefold rotation axes at 109° 23′ to each other | Simple<br>Body centered<br>Face centered | P<br>I<br>F |
| Tetragonal | $\alpha=\beta=\gamma=90^\circ$<br>$a=b\neq c$ | One fourfold rotation axis or one fourfold rotation–inversion axis | Simple<br>Body centered | P<br>I |
| Hexagonal | $\alpha=\beta=90^\circ$<br>$\gamma=120^\circ$<br>$a=b\neq c$ | One sixfold rotation axis or one sixfold axis rotation–inversion axis | Simple | P |
| Rhombohedral (trigonal) | $\alpha=\beta=\gamma\neq 90^\circ$<br>$a=b=c$ | One threefold rotation axis | Simple | R |
| Orthorhombic | $\alpha=\beta=\gamma=90^\circ$<br>$a\neq b\neq c$ | Any combination of three mutually perpendicular two-fold rotation axes or planes of symmetry | Simple<br>Body centered<br>Base centered<br>Face centered | P<br>I<br>C<br>F |
| Monoclinic | $\alpha=\gamma=90^\circ$<br>$\beta\neq 90^\circ$<br>$a\neq b\neq c$ | One twofold rotation axis or one twofold rotation–inversion axis | Simple<br>Base centered | P<br>C |
| Triclinic | $\alpha\neq\beta\neq\gamma\neq 90^\circ$<br>$a\neq b\neq c$ | None | Simple | P |

coordinates ($u'$, $v'$, $w'$) of any point on the line. The coordinates ($u'$, $v'$, $w'$) are not necessarily integers. However, by convention, ($u'$, $v'$, $w'$) are multiplied by the smallest number that produces integers $u$, $v$, and $w$. The crystal direction is described by putting the three integers in square brackets as $[uvw]$. $[uvw]$ are the indices of a specific crystal direction; each of the indices can take a value of positive or negative integer. All directions in a crystal that are symmetry equivalent to $[uvw]$ are represented by a notation with the integers in angular brackets as $\langle uvw\rangle$. For example, in a cubic crystal all diagonals of the unit cell are symmetry equivalent. So all the directions $[111]$, $[\bar{1}11]$, $[1\bar{1}1]$, $[11\bar{1}]$, $[\bar{1}\bar{1}1]$, $[\bar{1}1\bar{1}]$, $[1\bar{1}\bar{1}]$, and $[\bar{1}\bar{1}\bar{1}]$ can be represented by $\langle 111\rangle$. The bar over the number is for negative indices. Figure 1.4(a) shows some lattice directions and their indices in a unit cell.

The orientation of lattice planes can be described by using a set of three integers referred to as Miller indices. Miller indices are the reciprocal intercepts of the plane on the unit cell axes. If the crystal plane makes fractional intercepts of $1/h$, $1/k$, $1/l$ with

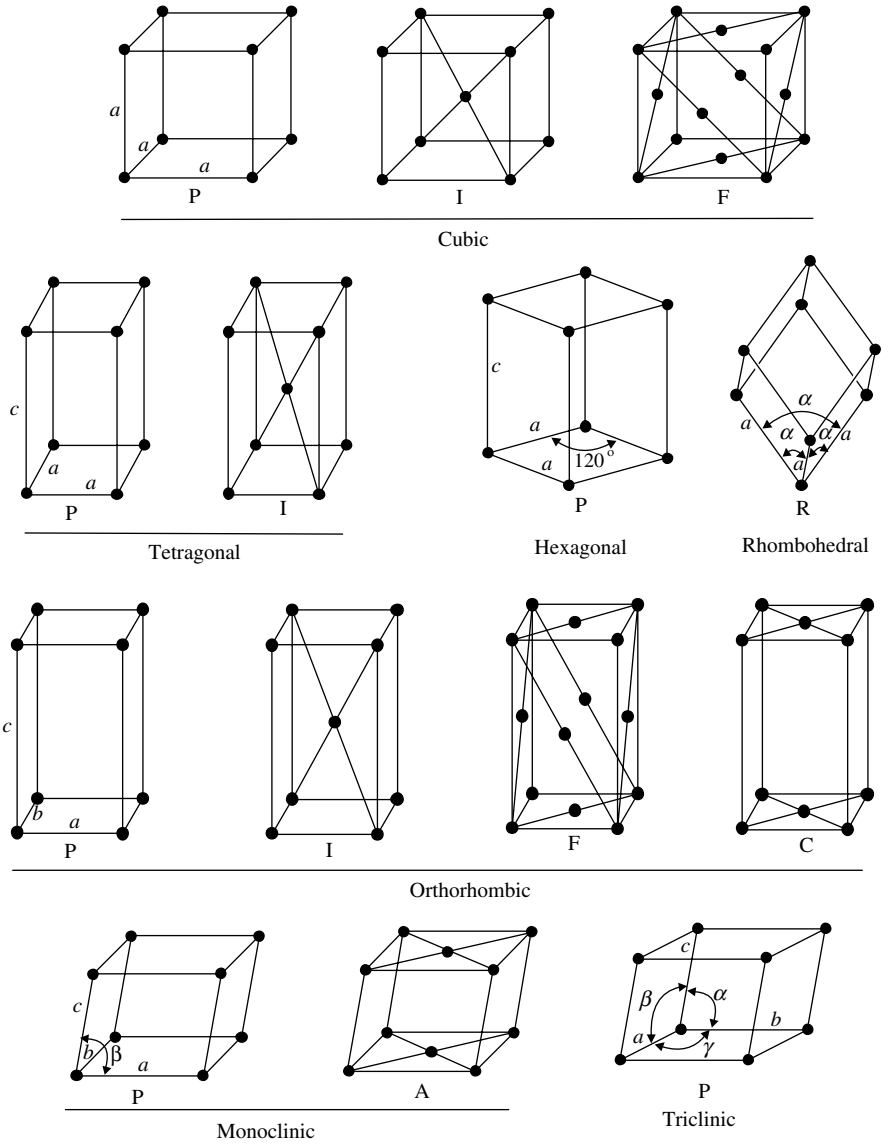


**FIGURE 1.3** Unit cells of the 14 Bravais lattices.

the three crystal axes, respectively, the Miller indices are (*hkl*). If plane runs parallel to an axis, intercept is at ∞, so Miller index is 0. Miller indices describe the orientation and spacing of a family of planes. Figure 1.4(b) shows some lattice planes and their Miller indices in a unit cell. The spacing between adjacent planes in a family is referred to as the "*d*-spacing." The symbol {*hkl*} refers to all planes that are symmetry

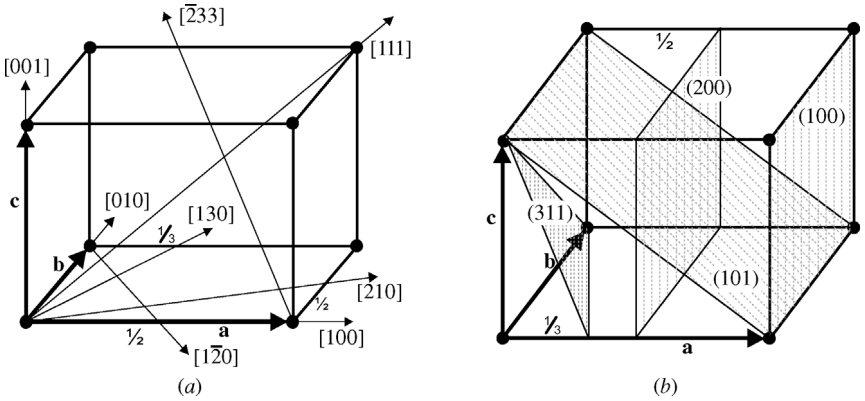


**FIGURE 1.4** (a) Indices of lattice directions and (b) Miller indices of lattice planes.

equivalent to (*hkl*). This group of equivalent planes is referred to as planes of a form. For the cubic system, all the planes (100), (010), (001), $(\bar{1}00)$, $(0\bar{1}0)$, and $(00\bar{1})$ belong to the form {100}. For a tetragonal crystal, $a = b \neq c$, only the first two indices imply the same interception distance on the crystal axes, so the form {100} would only include (100), (010), $(\bar{1}00)$, and $(0\bar{1}0)$.

Figure 1.5(a) shows the hexagonal unit cell and indices of some directions. It follows the same definition as other lattice types. However, lattice planes are often described by a different system of plane indexing, called Miller–Bravais indices. In hexagonal unit cells, it is common to use four axes coordinates, $\mathbf{a}_1$, $\mathbf{a}_2$, $\mathbf{a}_3$, and $\mathbf{c}$, in which $\mathbf{a}_1$, $\mathbf{a}_2$, and $\mathbf{a}_3$ are lying in the basal plane and $\mathbf{c}$ is perpendicular to

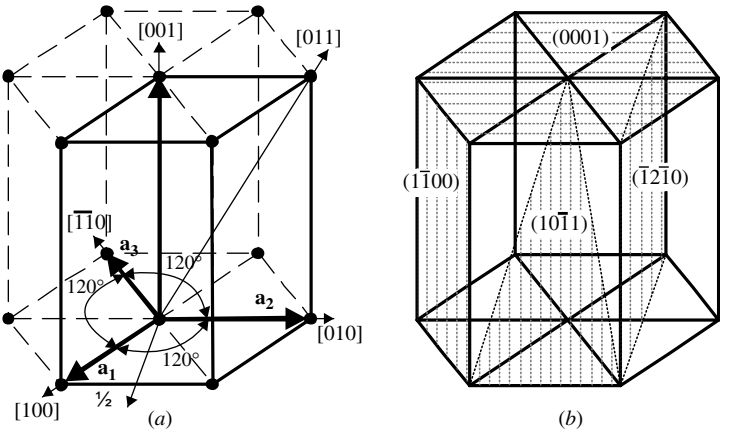


**FIGURE 1.5** (a) Hexagonal unit cell (heavy lines) and indices of some lattice directions and (b) Miller–Bravais indices of some lattice planes in the hexagonal lattice.

all three axes. The indices of a plane in the hexagonal system are written as (*hkil*). Figure 1.5(b) shows some lattice planes in a hexagonal lattice described by Miller– Bravais indices. Since $\mathbf{a}_1$, $\mathbf{a}_2$, and $\mathbf{a}_3$ are symmetry equivalent and 120° apart from each other, there are only two independent axes among them. So the first three values in the Miller–Bravais indices maintain the following relation:

$$h + k + i = 0 \tag{1.1}$$

Since all cyclic permutations of $h$, $k$, and $i$ are symmetry equivalent, $(10\bar{1}0)$, $(\bar{1}100)$, and $(0\bar{1}10)$ are equivalent.

A zone is defined as a set of nonparallel planes, which are all parallel to one axis. This axis is called the zone axis. Miller indices for all planes in a zone obey the relationship

$$hu + kv + lv = 0 \tag{1.2}$$

where [*uvw*] defines the zone axis and (*hkl*) are the miller indices of each plane in the zone. Figure 1.6 shows some of the crystal planes in the cubic lattice that belong to the [001] zone.

The distance between two adjacent planes with the same indices is called interplanar spacing or *d*-spacing, which is an important parameter in the Bragg law. The interplanar spacing $d_{hkl}$ is a function of both the plane indices (*hkl*) and the lattice parameters ($a$, $b$, $c$, $\alpha$, $\beta$, $\gamma$). The equations of *d*-spacings for all seven crystal systems are listed in Table 1.2. More equations on the unit cell volume and interplanar angles can be found in Appendix 3 of Ref. [2].

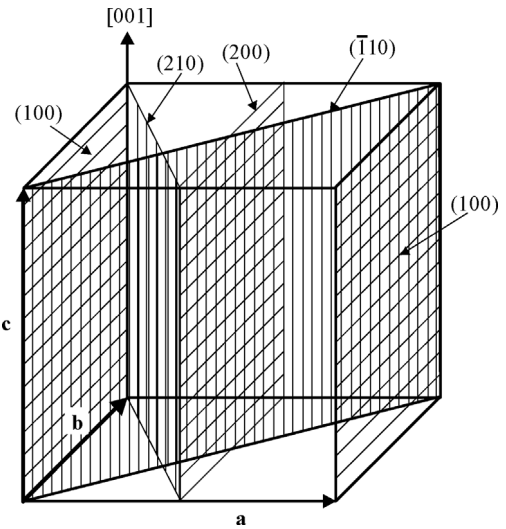


**FIGURE 1.6** All shaded crystal planes belong to [100] zone in the cubic lattice.

**TABLE 1.2 Equation of *d*-Spacing for All Seven Crystal Systems**

| Crystal System | Equation |
|---|---|
| Cubic | $\frac{1}{d_{hkl}^2} = \frac{h^2+k^2+l^2}{a^2}$ |
| Tetragonal | $\frac{1}{d_{hkl}^2} = \frac{h^2+k^2}{a^2} + \frac{l^2}{c^2}$ |
| Hexagonal | $\frac{1}{d_{hkl}^2} = \frac{4}{3}\left(\frac{h^2+hk+k^2}{a^2}\right) + \frac{l^2}{c^2}$ |
| Rhombohedral (trigonal) | $\frac{1}{d_{hkl}^2} = \frac{(h^2+k^2+l^2)\sin^2\alpha + 2(hk+kl+hl)(\cos^2\alpha - \cos\alpha)}{a^2(1 - 3\cos^2\alpha + 2\cos^3\alpha)}$ |
| Orthorhombic | $\frac{1}{d_{hkl}^2} = \frac{h^2}{a^2} + \frac{k^2}{b^2} + \frac{l^2}{c^2}$ |
| Monoclinic | $\frac{1}{d_{hkl}^2} = \frac{1}{\sin^2\beta}\left(\frac{h^2}{a^2} + \frac{k^2\sin^2\beta}{b^2} + \frac{l^2}{c^2} - \frac{2hl\cos\beta}{ac}\right)$ |
| Triclinic | $\frac{1}{d_{hkl}^2} = (1 - \cos^2\alpha - \cos^2\beta - \cos^2\gamma + 2\cos\alpha\cos\beta\cos\gamma)^{-1} \times \left(\frac{h^2}{a^2}\sin^2\alpha + \frac{k^2}{b^2}\sin^2\beta + \frac{l^2}{c^2}\sin^2\gamma + \frac{2kl}{bc}(\cos\beta\cos\gamma - \cos\alpha) + \frac{2lh}{ca}(\cos\gamma\cos\alpha - \cos\beta) + \frac{2hk}{ab}(\cos\alpha\cos\beta - \cos\gamma)\right)$ |

### 1.2.3 Atomic Arrangement in Crystal Structure

Actual crystal structures can be described by the Bravais lattice filled with the same or different kinds of atoms. The atoms take either the exact lattice points and/or points with fixed offset to the lattice points. The three most common crystal structures of metals are body-centered cubic (BCC), face-centered cubic (FCC), and hexagonal close-packed (HCP) structures as shown in Figure 1.7. BCC has two atoms per unit cell located at the coordinates (0, 0, 0) and $(\frac{1}{2}, \frac{1}{2}, \frac{1}{2})$, respectively. Many metals such as $\alpha$-iron, niobium, chromium, vanadium, and tungsten have BCC structure. FCC has four atoms per unit cells at the coordinates (0, 0, 0), $(0, \frac{1}{2}, \frac{1}{2})$, $(\frac{1}{2}, 0, \frac{1}{2})$, and $(\frac{1}{2}, \frac{1}{2}, 0)$, respectively. Metals with FCC structure include $\gamma$-iron, aluminum, copper, silver, nickel, and gold. HCP contains three equivalent hexagonal unit cells, each has two atoms at the coordinates (0, 0, 0) and $(\frac{2}{3}, \frac{1}{3}, \frac{1}{2})$ (or at equivalent position $(\frac{1}{3}, \frac{2}{3}, \frac{1}{2})$). Metals with HCP structure include beryllium, magnesium, zinc, and $\alpha$-titanium. Both FCC and HCP are close-packed arrangements. Both FCC (111) plane and HCP (0002) have the same atomic arrangement within the plane, but have different stacking sequences.

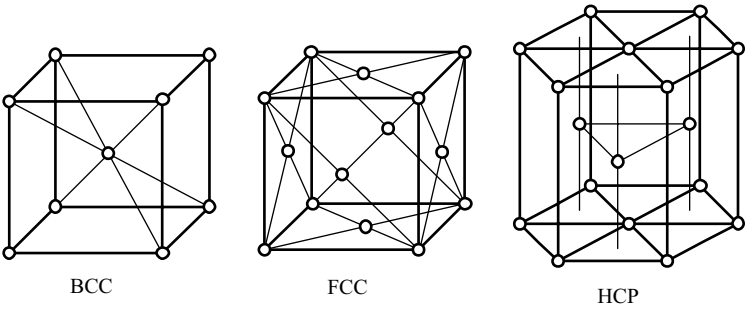


**FIGURE 1.7** Atomic arrangements in three common crystal structures of metals.

Structures of crystals formed by unlike atoms are built by the Bravais lattice with certain conditions. One is that the translation of the Bravais lattice must begin and end on the atoms of same kind. The other is that the space arrangement of each kind of atom possesses the same symmetry elements as the whole crystal. The structure of NaCl (rock salt) is shown in Figure 1.8. The unit cell of NaCl contains eight ions, located at the following coordinates:

- 4 $Na^+$ ions at (0, 0, 0), ($\frac{1}{2}$, $\frac{1}{2}$, 0), ($\frac{1}{2}$, 0, $\frac{1}{2}$), and (0, $\frac{1}{2}$, $\frac{1}{2}$);
- 4 $Cl^-$ ions at ($\frac{1}{2}$, $\frac{1}{2}$, $\frac{1}{2}$), (0, 0, $\frac{1}{2}$), (0, $\frac{1}{2}$, 0), and ($\frac{1}{2}$, 0, 0).

It can be seen that $Na^+$ ions form an FCC structure and four $Cl^-$ ions form an FCC with ($\frac{1}{2}$, $\frac{1}{2}$, $\frac{1}{2}$) translation from the $Na^+$ "lattice." Therefore, the Bravais lattice of NaCl crystal is face-centered cubic.

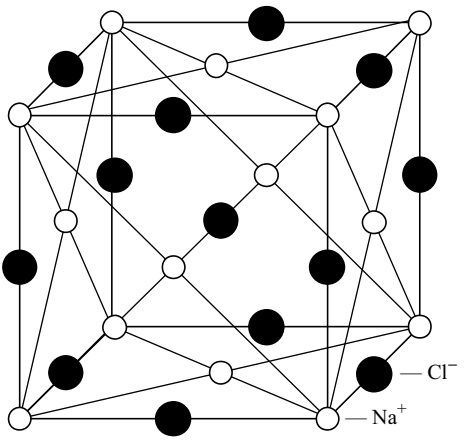


**FIGURE 1.8** The structure of NaCl. $Na^+$ is FCC and $Cl^-$ is FCC with ($\frac{1}{2}$, $\frac{1}{2}$, $\frac{1}{2}$) translation.

### 1.2.4 Imperfections in Crystal Structure

In the above, we have assumed that crystals have a very regular atomic arrangement following the crystal structure. However, most crystalline materials are not perfect. The regular pattern of atomic arrangement may be interrupted by crystal defects. There are various types of crystal defects, such as point defects, line defects, planar defects, and bulk defects.

Point defects are defects that involve randomly distributed extra or missing atoms. There is no strict definition of the size of a point defect, but generally a point defect is not extended in space in any dimension, but within a region of one or a few atoms. Vacancies are sites that should be occupied by an atom in a perfect crystal. Interstitials are extra atoms inserted between the normal atomic sites. Typically, interstitials are significantly smaller atoms compared to the matrix atoms in the crystal, for example, hydrogen, carbon, boron, or nitrogen atoms in metal crystals. Crystals with interstitials are also referred to as interstitial solid solutions. Substitutional solid solution contains another type of point defects—substitutional defects. In a substitutional solid solution of B in A, B atoms replace the sites normally occupied by A atoms. In a typical substitutional solution, B atoms are randomly distributed in the crystal. Under certain conditions, B atoms may replace A atoms in a regular pattern, called long-range order. The solution is then called ordered or superlattice structure. Point defects may change the lattice parameters in proportion to the concentration of the defects. Point defects play an important role in semiconductors.

Line defects are defects that extend in one dimension within a region of one or a few atoms in other two dimensions. Crystal dislocations are line defects. There are two basic types of dislocations, the edge dislocation and the screw dislocation. An edge dislocation is caused by the termination of a plane of atoms in the middle of a crystal or can be thought of as the result of adding or subtracting a half crystal plane between two adjacent full crystal planes. A screw dislocation is a line defect along which the atom arrangement is distorted like a screw thread or can be thought of as the result of cutting partway through the crystal and displacing it parallel to the edge of the cut. Dislocations can dramatically reduce the energy barrier to shearing a crystal along a crystal plane, so that the density of dislocations in a crystal can change the resistance of the crystal to plastic deformation.

Plane defects are crystal defects that extend in two dimensions and within a region of one or a few atoms in the third dimension. Grain boundaries are interfaces between contacting crystals that have different orientations. Depending on the degree of misorientation between the two contacting crystals, grain boundaries are categorized as low-angle grain boundaries and high-angle grain boundaries. The difference between low-angle grain boundary misorientation and high-angle grain boundary misorientation varies in the range of 10–15° depending on the material. The structure and property of low-angle grain boundaries have a strong dependence on the misorientation angle, while high-angle grain boundaries are not dependent on the misorientation. Antiphase boundaries are another type of plane defect existing in ordered alloys. The crystals on both sides of the boundary have the same structure and orientation with the interruption of the order by removing or adding a layer of atoms.

For example, if the ordering is in the sequence of ABABABAB, an antiphase boundary takes the form of ABABBABA or BABAABAB. Stacking faults are another type of plane defect. Stacking faults commonly occur in close-packed structures. The {111} planes of FCC and the {0002} planes of HCP have the same close-packed atomic planes with sixfold symmetry. Any two adjacent close-packed crystal planes in FCC and HCP are stacked in an identical sequence and labeled as AB. Each atom in B plane is directly on top of the center of triangles formed by three atoms in A plane. In HCP structure, the atomic location in third plane is directly above those of the first plane, so the stacking sequence continues as ABABABAB. In FCC structure, the atoms in the third layer fall on a location not directly above either A or B, but third location C. The atoms in the fourth plane are directly above those of A plane, so the sequence continues as ABCABCABC. A stacking fault is one or two plane deviations from the above perfect sequence. For example, ABCABCBCABCABC in FCC is a stacking fault and ABABABCABAB in HCP is a stacking fault. All plane defects disrupt the motion of dislocations through a material, so introducing the plane defects can change the mechanical properties of a material.

Bulk defects, also known as volume defects, are either clusters of the above defects or small regions of a different phase. The latter are often called precipitates. Bulk defects are obstacles to dislocation motion, so they are one of the mechanisms for strengthening materials. A crystal may contain many small regions or blocks with identical lattice structure, but separated by faults and dislocation clusters, as shown in Figure 1.9. The adjacent blocks are slightly disoriented so that the perfect crystal lattice extends only within each block. This kind of structure is referred to as a mosaic structure. The extent of the mosaic structure is also described as mosaicity. A crystal with low mosaicity means it has larger perfect crystal blocks or smaller misorientation between blocks.

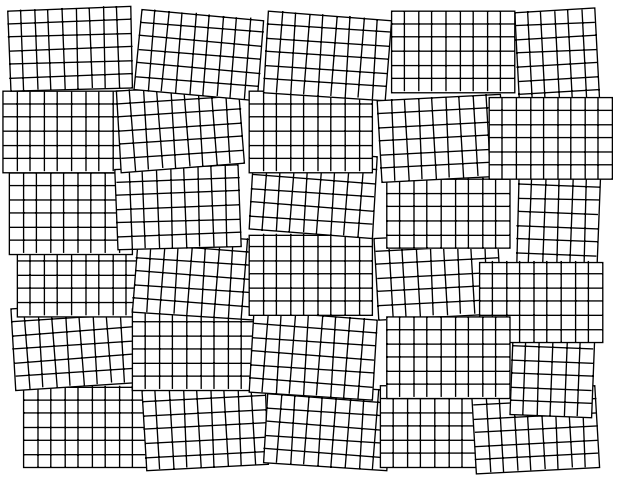

**FIGURE 1.9** Illustration of crystallite mosaic in a crystal.

## 1.3 PRINCIPLES OF X-RAY DIFFRACTION

X-rays are electromagnetic radiation with a wavelength in the range of 0.01–100 Å. X-rays belong to a portion of the electromagnetic spectrum overlapping with gamma rays in the shorter wavelengths and with ultraviolet in the longer wavelengths. The wavelength of typical X-rays used in X-ray diffraction is in the vicinity of 1 Å, which is comparable to the range of interatomic spacing in crystals. When a monochromatic X-ray beam hits a sample, in addition to absorption and other phenomena, it generates scattered X-rays with the same wavelength as the incident beam. This type of scattering is also known as elastic scattering or coherent scattering. The scattered X-rays from a sample are not evenly distributed in space, but a function of the electron distribution in the sample. The atomic arrangement in the sample can be ordered like a single crystal or disordered like glass or liquid. As such, the intensities and spatial distributions of the scattered X-rays form a specific diffraction pattern that is uniquely determined by the structure of the sample.

### 1.3.1 Bragg Law

There are many theories and equations about the relationship between the diffraction pattern and the material structure. Bragg law is a simple way to describe the diffraction of X-rays by a crystal. In Figure 1.1(a), the incident X-rays hit the crystal planes with an incident angle $\theta$ and reflection angle $\theta$. The diffraction peak is observed when the Bragg condition is satisfied:

$$n\lambda = 2d\sin\theta \tag{1.3}$$

where $\lambda$ is the wavelength, $d$ is the distance between each adjacent crystal planes ($d$-spacing), $\theta$ is the Bragg angle at which one observes a diffraction peak, and $n$ is an integer number, called the order of reflection. That means that the Bragg condition with the same $d$-spacing and $2\theta$ angle can be satisfied by various X-ray wavelengths (energies). The first-order reflection ($n = 1$) is from the fundamental energy, and the second- or third-order reflections are from harmonic energies two or three times the fundamental energy.

In X-ray diffraction using a single wavelength, the Bragg equation is typically expressed with $n = 1$ for the first order of diffraction because the higher order reflections can be considered as being from different lattice planes. For instance, the second-order reflection from ($hkl$) planes is equivalent to the first-order reflection from ($2h$, $2k$, $2l$) planes. The diffraction peak is displayed as diffracted intensities at a range of $2\theta$ angles. For perfect crystals with perfect instrumentation, the peak is a delta function (the dark straight vertical line) as shown in Figure 1.10(b). The intensity is denoted by $I$.

The delta function is an oversimplified model that requires a perfect crystal without mosaic structure and a perfectly collimated monochromatic X-ray beam. A typical diffraction peak is a broadened peak displayed by the curved line in Figure 1.10(b). The peak broadening can be due to many effects, including imperfect crystal conditions, such as strain, mosaic structure, and finite size; ambient conditions, such as atomic thermal vibration; and instrumental conditions, such as X-ray beam size,

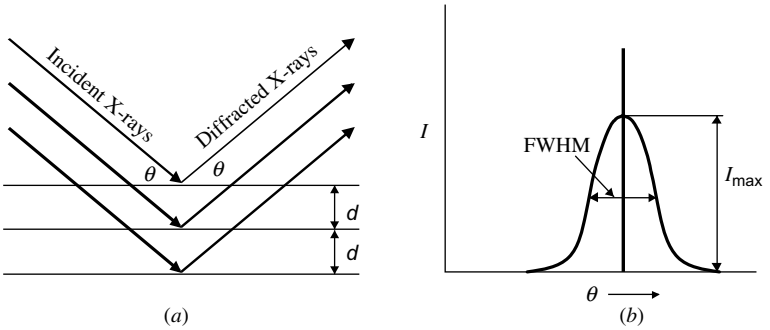


**FIGURE 1.10** The incident X-rays and reflected X-rays make an angle of $\theta$ symmetric to the normal of crystal plane (a). The diffraction peak is observed at the Bragg angle $\theta$ (b).

beam divergence, beam spectrum distribution, and detector resolution. The curved line gives a peak profile, which is the diffracted intensity distribution in the vicinity of the Bragg angle. The highest point on the curve gives the maximum intensity of the peak, $I_{max}$. The width of a peak is typically measured by its full width at half maximum (FWHM). The total diffracted energy of a diffracted beam for a peak can be measured by the area under the curve, which is referred to as integrated intensity. The integrated intensity is a more consistent value for measuring the diffracted intensity of a reflection since it is less affected by all the peak broadening factors. Causes of peak broadening, while increasing FWHM, typically also reduce the maximum intensity at the same time. Therefore, overall variation of the integrated intensity is less significant compared to the variations of FWHM and $I_{max}$.

### 1.3.2 Diffraction Patterns

The above diffraction condition is based on the existence of long periodicity of crystalline materials. In general, X-ray diffraction can provide information on the atomic arrangement in materials with long-range order, short-range order, or no order at all, like gases, liquids, and amorphous solids. A material may have one of the above atomic arrangement types, or a mixture of the above types. Figure 1.11 gives a schematic comparison of diffraction patterns for crystalline solids, liquids, amorphous solids, and monatomic gases as well as their mixtures. The diffraction pattern from crystals has many sharp peaks corresponding to various crystal planes based on the Bragg law. The peaks at low $2\theta$ angles are from crystal planes of large $d$-spacing and vice versa at high $2\theta$ angles. To satisfy the Bragg condition at all crystal planes, the crystal diffraction pattern is actually generated from polycrystalline materials or powder materials. Therefore, the diffraction pattern is also called powder diffraction pattern. A similar diffraction pattern can be collected with a single crystal if the crystal has been rotated at various angles during the data collection so that the Bragg law can be satisfied when the crystal is at the right orientation. The techniques have been used in the Gandolfi camera in which the crystal is rotated above an axis tilted 45° from the camera axis. The powder-like

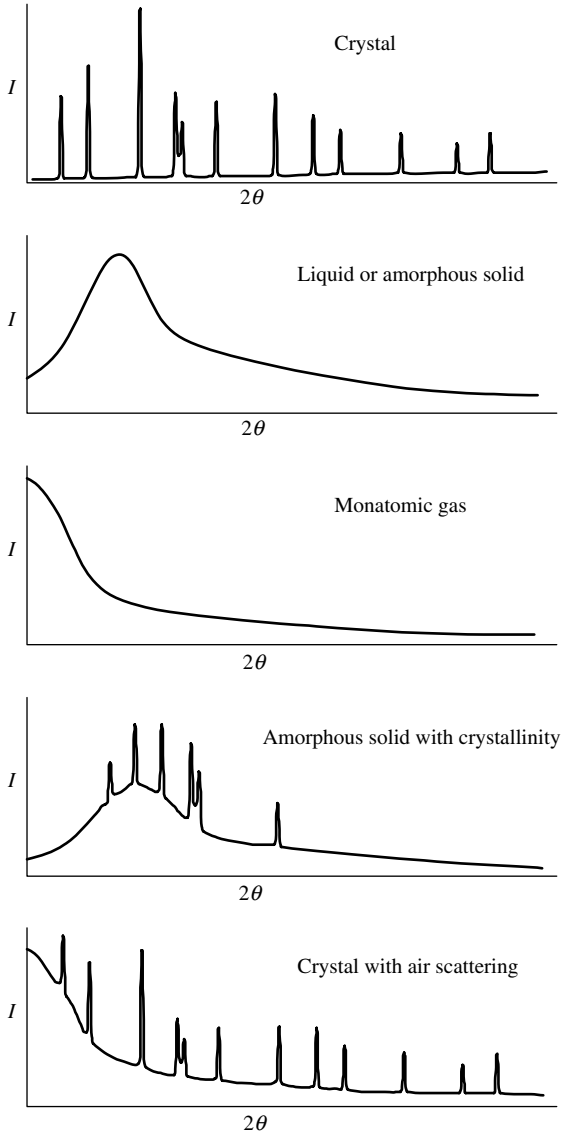


**FIGURE 1.11** Diffraction patterns from crystalline solids, liquids, amorphous solids, and monatomic gases as well as their mixtures.

pattern generated by rotating a single-crystal sample with other types of diffractometers is also referred to as Gandolfi pattern.

Both amorphous solid and liquid materials do not have the long-range order as a crystal does, but the atomic distance has a narrow distribution due to the atoms being tightly packed. In this case, the intensity of the scattered X-rays forms one or two maxima with a very broad distribution in the $2\theta$ range. The intensity versus $2\theta$

distribution reflects the distribution of the atomic distances. In principle, a pattern like this should be called a scattering pattern since there is no diffraction as we have defined earlier, but we may call it diffraction pattern for convenience. A monatomic gas has no order at all. The atoms are distributed randomly in space. The scattering curve shows no feature at all except that the scattered intensity drops continuously with the increase of the $2\theta$ angle. The scattering curve for air or gas shows a similar feature although the molecules have a preferred distance between atoms within each molecule. The diffraction pattern from a material containing both amorphous and crystalline solids has a broad background from the amorphous phase and sharp peaks from crystalline phase. For example, many polymer materials have an amorphous matrix with crystallized regions. The diffraction pattern may contain air-scattering background in addition to sharp diffraction peaks. The air scattering can be generated from the incident beam or diffracted beam. If the air scattering is not removed by the diffractometer, the diffraction pattern contains a high background at low $2\theta$ angle and the background gradually decreases with increasing $2\theta$ angle.

## 1.4 RECIPROCAL SPACE AND DIFFRACTION

The Bragg law gives a simple relationship between the diffraction pattern and the crystal structure. Many X-ray diffraction applications can be easily explained by the Bragg law. X-ray diffraction phenomena can also be explained in reciprocal space by the reciprocal lattice and the Ewald sphere. X-ray diffraction analysis with concepts in reciprocal space is a powerful way of understanding and solving many diffraction problems [2–5].

### 1.4.1 Reciprocal Lattice

Reciprocal lattice is a transformation of the crystal lattice in real space to reciprocal space. The shape and size of a unit cell in real space can be defined by three vectors **a**, **b**, and **c** all starting from any single lattice point. The unit cell of the corresponding reciprocal lattice is then given by three vectors $\mathbf{a}^*$, $\mathbf{b}^*$, and $\mathbf{c}^*$ (also referred to as reciprocal lattice axes), and

$$\begin{aligned} \mathbf{a}^* &= \frac{1}{V}(\mathbf{b} \times \mathbf{c}), \\ \mathbf{b}^* &= \frac{1}{V}(\mathbf{c} \times \mathbf{a}), \\ \mathbf{c}^* &= \frac{1}{V}(\mathbf{a} \times \mathbf{b}) \end{aligned} \tag{1.4}$$

where $V$ is the volume of the crystal unit cell in the real space and

$$V = \mathbf{a} \cdot \mathbf{b} \times \mathbf{c} \tag{1.5}$$

Since each reciprocal lattice axis is the vector product of two lattice axes in real space, it is perpendicular to the planes defined by the two lattice axes. The original

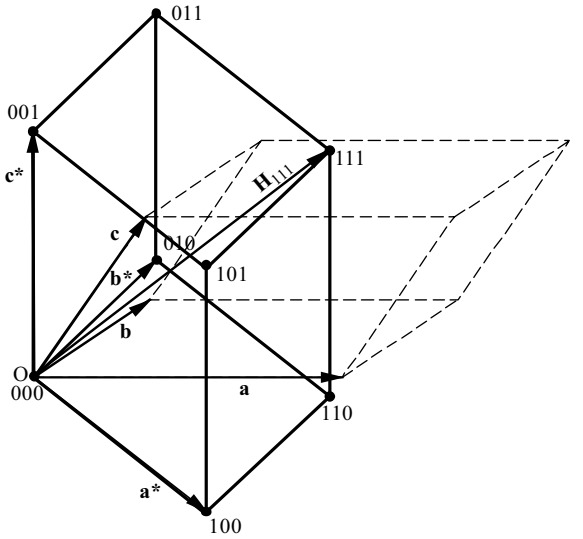


**FIGURE 1.12** The relationship between the original lattice in real space and the reciprocal lattice.

lattice axes and reciprocal lattice axes maintain the following relations:

$$\mathbf{a} \cdot \mathbf{a}^* = \mathbf{b} \cdot \mathbf{b}^* = \mathbf{c} \cdot \mathbf{c}^* = 1 \tag{1.6}$$

and

$$\mathbf{b} \cdot \mathbf{a}^* = \mathbf{c} \cdot \mathbf{a}^* = \mathbf{a} \cdot \mathbf{b}^* = \mathbf{c} \cdot \mathbf{b}^* = \mathbf{b} \cdot \mathbf{c}^* = \mathbf{a} \cdot \mathbf{c}^* = 0 \tag{1.7}$$

Figure 1.12 illustrates the relationship between the original lattice in real space and the reciprocal lattice. The unit cell of the original lattice is drawn in dotted lines. The three reciprocal lattice axes define a unit cell of the reciprocal lattice (solid lines). The origin of the reciprocal lattice axes, denoted by O, is the origin of the reciprocal lattice. The repeat translation of the reciprocal lattice unit cell in three dimensions forms the complete reciprocal lattice. Except the origin, each lattice point is denoted by a set of three integers (*hkl*), which are the number of translations of the three reciprocal lattice axes, respectively, to reach the lattice point. In other words, the vector drawn from the origin to the lattice point (*hkl*) is given by

$$\mathbf{H}_{hkl} = h\mathbf{a}^* + k\mathbf{b}^* + l\mathbf{c}^* \tag{1.8}$$

and the direction of the vector $\mathbf{H}_{hkl}$ is normal to the lattice planes (*hkl*) in real space. The magnitude of the vector $\mathbf{H}_{hkl}$ is given by the *d*-spacing of the (*hkl*) planes:

$$|\mathbf{H}_{hkl}| = \frac{1}{d_{hkl}} \tag{1.9}$$

Therefore, each point (*hkl*) in the reciprocal lattice represents a set of lattice planes (*hkl*) in the real space lattice. The position of the point in the reciprocal lattice

defines the orientation and $d$-spacing of the lattice planes in the real space lattice. The farther away a reciprocal lattice point is from the origin, the smaller is the $d$-spacing of the corresponding lattice planes. For example, the reciprocal lattice point (111) represents the (111) lattice planes in the real space lattice, and the lattice vector is given by

$$\mathbf{H}_{111} = \mathbf{a}^* + \mathbf{b}^* + \mathbf{c}^*$$

and

$$d_{111} = \frac{1}{|\mathbf{H}_{111}|} = \frac{1}{|\mathbf{a}^* + \mathbf{b}^* + \mathbf{c}^*|}$$

### 1.4.2 The Ewald Sphere

The relationship between the Bragg condition and the reciprocal lattice can be explained visually by the Ewald sphere, also referred to as reflection sphere. Ewald came up with a geometrical construction to help visualize which Bragg planes are in the correct orientation to diffract. In Figure 1.13, the diffracting crystal is located in the center of the Ewald sphere, C. The radius of the Ewald sphere is defined as $1/\lambda$. The incident beam can be visualized as the vector from I to C, and the diffracted beam is the vector from C to P. Both the incident beam and diffracted beam are at an angle $\theta$ from a set of crystal planes ($hkl$). The $d$-spacing of the crystal planes is . In the Ewald sphere, both incident beam vector $\mathbf{s}_0/\lambda$ and diffracted beam vector $\mathbf{s}/\lambda$ start at the point C and end at points O and P, respectively. The vector from O to P is the reciprocal lattice vector $\mathbf{H}_{hkl}$ and is perpendicular to the crystal planes. The three vectors have the following relationship:

$$\frac{\mathbf{s} - \mathbf{s}_0}{\lambda} = \mathbf{H}_{hkl} = h\mathbf{a}^* + k\mathbf{b}^* + l\mathbf{c}^* \tag{1.10}$$

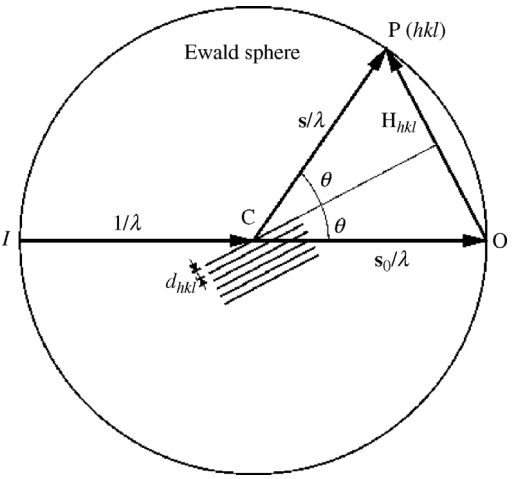


**FIGURE 1.13** The Ewald sphere and Bragg condition in reciprocal space.

and the magnitude of the vectors has the following relationship based on the Bragg law:

$$\left|\frac{\mathbf{s}-\mathbf{s}_0}{\lambda}\right| = \frac{2\sin\theta}{\lambda} = |\mathbf{H}_{hkl}| = \frac{1}{d_{hkl}} \tag{1.11}$$

The point O is the origin of the reciprocal lattice and the point P is the reciprocal point (*hkl*). The Bragg condition is satisfied only when the reciprocal lattice point falls on the Ewald sphere. For a single crystal, the chance to have a reciprocal lattice point on the Ewald sphere is very small if the crystal orientation is fixed. Multiplying both ends of Eq. (1.10) by the three lattice axes in real space, respectively, we obtain the Laue equations

$$\begin{aligned} \mathbf{a}\cdot(\mathbf{s}-\mathbf{s}_0) &= h\lambda \\ \mathbf{b}\cdot(\mathbf{s}-\mathbf{s}_0) &= k\lambda \\ \mathbf{c}\cdot(\mathbf{s}-\mathbf{s}_0) &= l\lambda \end{aligned} \tag{1.12}$$

The Laue equations establish that a periodic three-dimensional lattice produces diffraction maxima at specific angles depending on the incident beam direction and the wavelength. The Laue equations are suitable to describe the diffraction geometry of a single crystal. The Bragg law is more conveniently used for powder diffraction. Both the Laue equations and the Bragg law define the diffraction condition in different formats.

The distance between the origin of the reciprocal lattice (O) and the lattice point (P) is reciprocal to the *d*-spacing. The largest possible magnitude of the reciprocal lattice vector is given by $2/\lambda$. This means that the smallest *d*-spacing satisfying the Bragg condition is $\lambda/2$. In powder X-ray diffraction, the random orientation of all crystallites can take all possible orientations assuming an infinite number of crystallites in diffraction. The trace of the reciprocal lattice points from all crystallites can be considered as a series of spherical surfaces with the origin O as the center. Therefore, the condition for satisfying the Bragg law is only if the *d*-spacing is greater than half of the wavelength. In other words, the Bragg condition can be satisfied if a reciprocal lattice point falls in a sphere of $2\lambda$ from the origin O. This sphere is called the limiting sphere for powder diffraction. Figure 1.14 illustrates the limiting sphere for powder diffraction in a two-dimensional cut through the origin. All the reciprocal lattice points within the limiting sphere are denoted by black dots. For powder samples, all the reciprocal lattice points having the same distance from the origin form a sphere shown by a circle of broken line. For example, the reciprocal lattice point P(*hkl*) would not fall on the Ewald sphere for a single crystal with fixed orientation. But for powder samples, the equivalent reciprocal lattice point from some crystallites would fall on the Ewald sphere at point P′. The same explanation can also be given for rotating single crystal. In this case, the reciprocal lattice point P(*hkl*) can cross with the Ewald sphere by a proper rotation. The Gandolfi camera works in this principle.

### 1.4.3 Diffraction Cone and Diffraction Vector Cone

In powder diffraction, for a fixed incident X-ray vector $\mathbf{s}_0/\lambda$, the diffracted beam vector $\mathbf{s}/\lambda$ takes all directions at a $2\theta$ angle from the incident beam direction, as shown

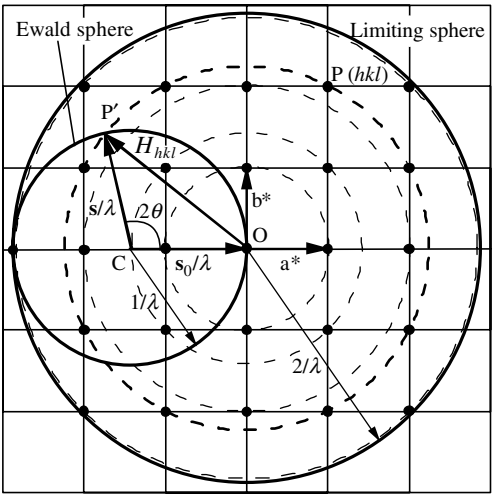


**FIGURE 1.14** Limiting sphere for the powder diffraction.

in Figure 1.15. The end of $\mathbf{s}/\lambda$ vector forms a circle on the Ewald sphere passing through the reciprocal lattice point P($hkl$), P′($hkl$), and all equivalent reciprocal lattice points. The diffracted beams form a cone with the incident beam on the rotation axis. This cone is referred to as diffraction cone. The $2\theta$ angle can take values from 0 to

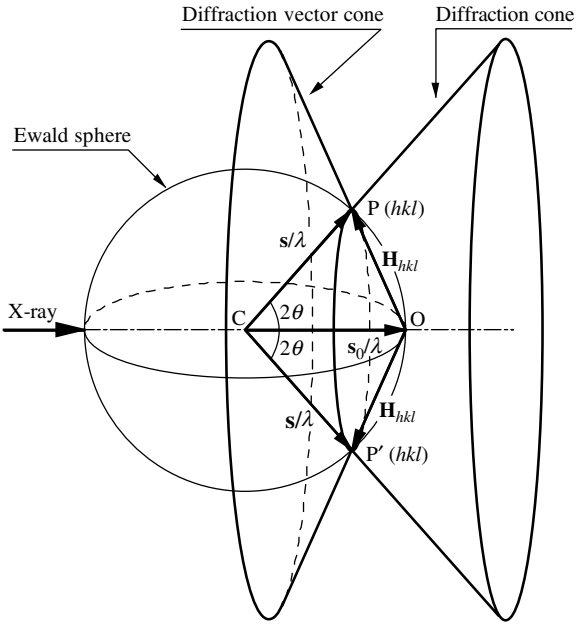


**FIGURE 1.15** Diffraction cone and diffraction vector cone illustrated on the Ewald sphere.

180°, corresponding to all the directions of the diffracted beams. The diffraction vector $\mathbf{H}_{hkl}$, starting from the origin of the reciprocal lattice (O) to the trace circle of the lattice point P(*hkl*) and equivalents, also forms a cone, named the diffraction vector cone. The angle between the diffraction vector and the incident beam is $90° - \theta$. In the illustration with the Ewald sphere, the diffraction cone and the diffraction vector cone start from different points. In real space geometry, both the diffraction cone and the diffraction vector cone are considered as starting from the same point (the sample location or instrument center).

## 1.5 TWO-DIMENSIONAL X-RAY DIFFRACTION

### 1.5.1 Diffraction Pattern Measured by Area Detector

The diffraction patterns shown in Figure 1.11 are displayed as diffracted intensity versus $2\theta$ angle assuming that the diffracted intensity is a unique function of diffraction angle. The actual diffraction pattern is distributed in the 3D space around the diffracting sample. Figure 1.16 illustrates the diffraction patterns from single-crystal and polycrystalline samples. The diffracted beams from a single crystal point to discrete directions, each corresponding to a family of diffracting planes, as shown in Figure 1.17. Each diffracted beam is a direct reflection of the incident X-ray beam based on the Bragg law. The diffracted beams are intercepted by an area detector and the X-ray intensity distribution on the sensing area is converted to an image-like diffraction pattern, also referred to as a frame. The region representing each diffracted beam in the frame is called diffraction spot. Figure 1.16(b) is a diffraction frame from a single crystal of chicken egg white lysozyme. Due to the large and complex unit cell of this protein crystal, there are many diffraction spots in the frame. Today, in the area of single-crystal diffraction, two-dimensional detectors are required to collect enough diffraction data to solve the structure of a complex crystal. Single-crystal X-ray diffraction has been covered by much literature [9,10]. This book will mainly cover diffractions from polycrystalline materials or other non-single-crystal materials in the following chapters.

Polycrystalline materials consist of many crystalline domains, ranging from a few to more than a million in the incident beam. In single-phase polycrystalline materials, all these domains have the same crystal structure but various orientations. Polycrystalline materials can also be multiphase materials with more than one kind of crystal structure blended together. Polycrystalline materials can also be mixed or bonded to different materials such as thin films or coatings on single-crystal substrates. The crystalline domains can be embedded in an amorphous matrix. Most often, the sample undergoing X-ray analysis is not a randomly oriented polycrystalline material, but a combination of polycrystalline, amorphous, and single-crystal contents, polycrystalline with preferred orientation, or deformed due to residual stresses. The diffracted beams from a polycrystalline (powder) sample form a series diffraction cone in 3D space since a large number of crystals oriented randomly in the space are covered by the incident X-ray beam, as shown in

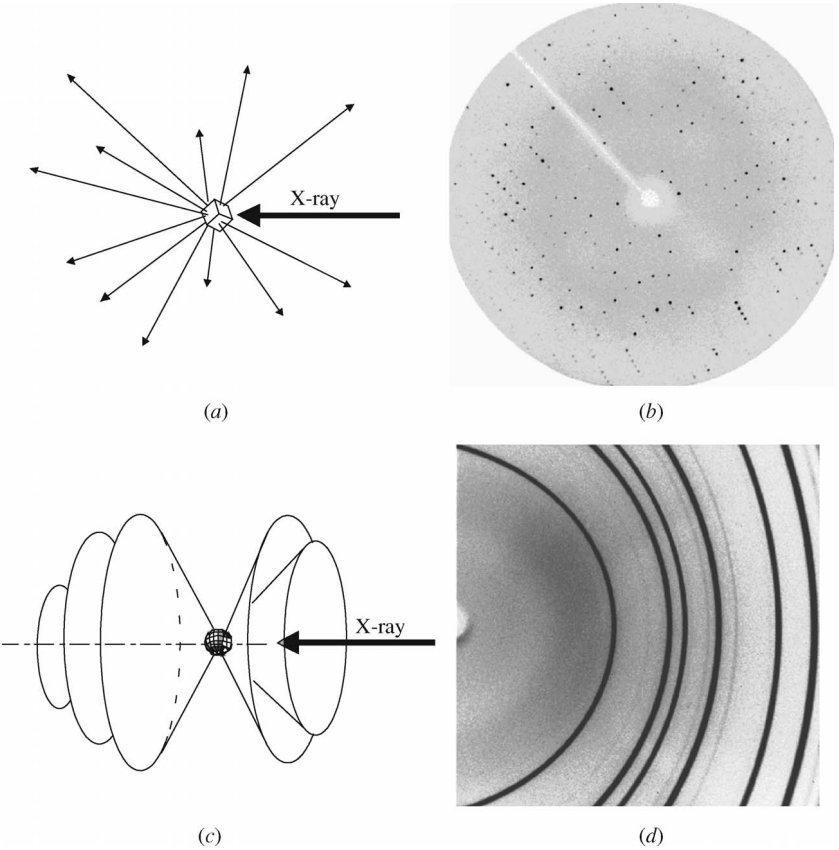


**FIGURE 1.16** The patterns of diffracted X-rays: (a) from a single crystal, (b) diffraction frame from a lysozyme protein single crystal, (c) diffraction cones from a polycrystalline sample, and (d) a diffraction frame from corundum powder.

Figure 1.16(c). Each diffraction cone corresponds to the diffraction from the same family of crystalline planes in all the participating grains. The diffraction frame from a polycrystalline sample is a cross section of the detecting plane and the diffraction cones. Figure 1.16(d) is a diffraction frame collected from corundum powder with an area detector. Since the diffraction pattern collected with an area detector is typically given as a two-dimensional image frame, the X-ray diffraction with an area detector is called two-dimensional diffraction.

### 1.5.2 Two-Dimensional X-Ray Diffraction System and Major Components

Two-dimensional X-ray diffraction ($XRD^2$) systems have a variety of configurations and component options to fulfill requirements of different samples and applications. As shown in Figure 1.17, a typical $XRD^2$ system normally consists of five basic components:

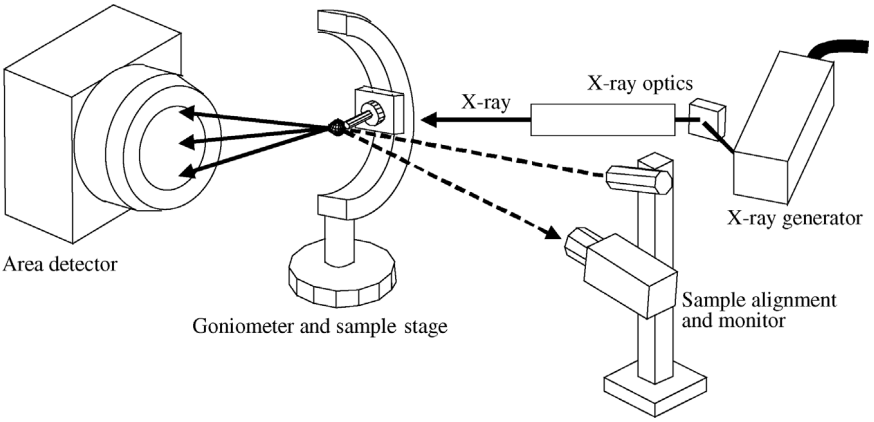


**FIGURE 1.17** Five basic components in an XRD$^2$ system: X-ray source (sealed tube generator); X-ray optics (monochromator and collimator); goniometer and sample stage; sample alignment and monitor (laser video); and area detector.

- *X-Ray Source:* produces X-rays with the required radiation energy, focal spot size, and intensity;
- *X-Ray Optics:* conditions the primary X-ray beam to the required wavelength, beam focus size, beam profile, and divergence;
- *Goniometer and Sample Stage:* establishes and maneuvers the geometric relationship between primary beam, sample, and detector;
- *Sample Alignment and Monitor:* assists users with positioning the sample into the instrument center and monitors the sample state and position;
- *Area Detector:* intercepts and records the scattering X-rays from a sample, and saves and displays the diffraction pattern into a two-dimensional frame.

Each of the basic components may have several options suitable for various application and functions. The whole system is controlled by a computer with software for instrument control, data acquisition, and data analysis. In addition to the five basic components, there are some other accessories, such as a low-temperature stage, high-temperature stage, helium or vacuum beam path for SAXS, beam stop, and alignment and calibration fixtures. The geometry conventions, X-ray source and optics, detector, goniometer, sample stage, and various configurations will be covered in the following chapters.

### 1.5.3 Summary

A two-dimensional diffraction frame contains far more information than a diffraction pattern measured with conventional diffraction system with a point detector or a linear position-sensitive detector. The speed of two-dimensional diffraction is typically several orders of magnitude higher than conventional diffraction. Two-dimensional

X-ray diffraction analyses, commonly performed on polycrystalline materials, include phase identification, quantitative phase analysis, preferred orientation, and residual stresses.

Phase identification (phase ID) can be done by integration in the selected $2\theta$ range along the Debye rings. The integrated data give better intensity and statistics for phase ID and quantitative analysis, especially for those samples with texture, large grain size, or small quantity. Then the integrated diffraction profiles can be analyzed with existing algorithms and methods, profile fitting with conventional peak shapes and fundamental parameters, quantification of phases, and lattice parameter indexing and refinement. The diffraction results can be used to search and match with the ICDD database [11–16].

Texture measurement with two-dimensional diffraction is extremely fast compared to measurement using a point or linear detector. The area detector collects texture data and background values simultaneously for multiple poles and multiple directions. Due to the high measurement speed, pole figures can be measured at very fine steps, allowing detection of very sharp textures [17,18].

Stress measurement using the area detector is based on a direct relationship between the stress tensor and diffraction cone distortion. Since the whole or a part of the Debye ring is used for stress calculation, two-dimensional diffraction can measure stress with high sensitivity, high speed, and high accuracy. It is very suitable for samples with large crystals and textures. Simultaneous measurement of stress and texture is also possible since 2D data consist of both stress and texture information [19–21].

Percent crystallinity can be measured faster and more accurately with data analysis over 2D frames, especially for samples with anisotropic distribution of crystalline orientation. The amorphous region can be defined externally within user-defined regions, or the amorphous region can be defined with the crystalline region included when the crystalline region and the amorphous region overlap.

SAXS data can be collected at high speed. Anisotropic features from specimens, such as polymers, fibrous materials, single crystals, and biomaterials, can be analyzed and displayed in two dimensions. Desmearing correction is not necessary due to the collimated point X-ray beam. Since one exposure takes all the required SAXS information, it is easy to scan over the sample to map the structure information from small-angle diffraction [22,23].

Microdiffraction data are collected with speed and accuracy. X-ray diffraction from small sample amounts or small sample areas has always been a slow process because of limited beam intensity. The 2D detector captures whole or a large portion of the diffraction rings, so spotty, textured, or weak diffraction data can be integrated over the selected diffraction rings [24–26].

Thin film samples with a mixture of single crystals, random polycrystalline layers, and highly textured layers can be measured with all the features appearing simultaneously in diffraction frames. The pole figures from different layers and substrates can be overlapped to reveal the orientation relationship [27–29]. The use of an area detector can dramatically speed up the data collection for reciprocal space mapping on an in-plane reciprocal lattice point [30].

Combinatorial screening by two-dimensional X-ray diffraction is one of the most powerful high-throughput screening techniques. Because of the penetrating power of